

## SUPPLEMENTAL FIGURE LEGENDS

**Supplemental Figure 1, related to Figure 1.** *PIGR* mRNA expression across cancer types and confirmation of dimeric fraction in native IgA antibodies. (A) TCGA data showing *PIGR* mRNA expression, expressed as RNA Seq V2 RSEM ( $\log_2(\text{value}+1)$ ) in several epithelial and non-epithelial malignancies. (B) Native human IgA was subjected to mass spectrometry. Two unique peptides, one is from amino acid 47 to 58 (SSEDPNEDIVER) and the other from amino acid 61-69 (IIVPLNNR), of human J-chain were identified. (C) Native gel electrophoresis of two different lot of native human IgA procured from Abcam (ab91025) which shows the presence of both dimeric and monomeric IgA in the gel at their corresponding molecular weights.

**Supplemental Figure 2, related to Figures 1 and 6.** Production and purification of KRAS<sup>G12D</sup> and IDH1<sup>R132H</sup> mutation specific recombinant dIgA1 and IgG4 antibodies. (A) Immunoblots using denatured lysates of transduced HEK293T cells confirming expression of alpha ( $\alpha$ ) or gamma ( $\gamma$ ) heavy chain, kappa ( $\kappa$ ) light chain, specific for KRAS<sup>G12D</sup> or IDH1<sup>R132H</sup> dIgA1 or IgG4, and J-chain for dimeric IgA1 ( $n=3$ ). (B) Graphs showing peaks of purified anti-human KRAS<sup>G12D</sup> and IDH1<sup>R132H</sup> dIgA and IgG4 antibodies at 280nm. (C) Native gel electrophoresis of different IgA antibodies that shows the presence of dimeric (*black arrows*) and monomeric IgA (*red arrows*) in the gel at their corresponding molecular weights. (D) Immunoblots showing that recombinant anti-KRAS<sup>G12D</sup>-IgA1 and anti-KRAS<sup>G12D</sup>-IgG4 antibodies specifically recognize mutant KRAS<sup>G12D</sup>, in the lysates of KRAS<sup>G12D</sup>-PAmCherry-OVCAR3, but not KRAS<sup>WT</sup>-PAmCherry-OVCAR3 cells, as well as KRAS<sup>G12D</sup> mutated A427 and SK-LU-1 lung cancer cell lines. Anti-mCherry antibody recognized KRAS<sup>WT</sup>-PAmCherry and KRAS<sup>G12D</sup>-PAmCherry fusion proteins in transduced

OVCAR3 lysates ( $n=3$ ). (E) Immunoblots showing KRAS<sup>G12D</sup> levels in anti-KRAS<sup>G12D</sup>-IgA1/IgG4 or non-antigen specific irrelevant IgA-treated KRAS<sup>G12D</sup>-A427 lung cancer cell lysates. (F) Transcytosis experiment adding biotinylated anti-KRAS<sup>G12D</sup>-IgA1/IgG4 or irrelevant IgA to the upper chamber of a transwell system, where physical access of antibodies to the basal chamber is prevented by WT or KRAS<sup>G12D</sup>-OVCAR3 cells grown to confluence in transwell inserts. Dot blots showing presence of KRAS<sup>G12D</sup> (*left panel*), human IgA (*middle panel*), or human IgG (*right panel*) in the streptavidin immunoprecipitates of the basal and upper chamber contents.

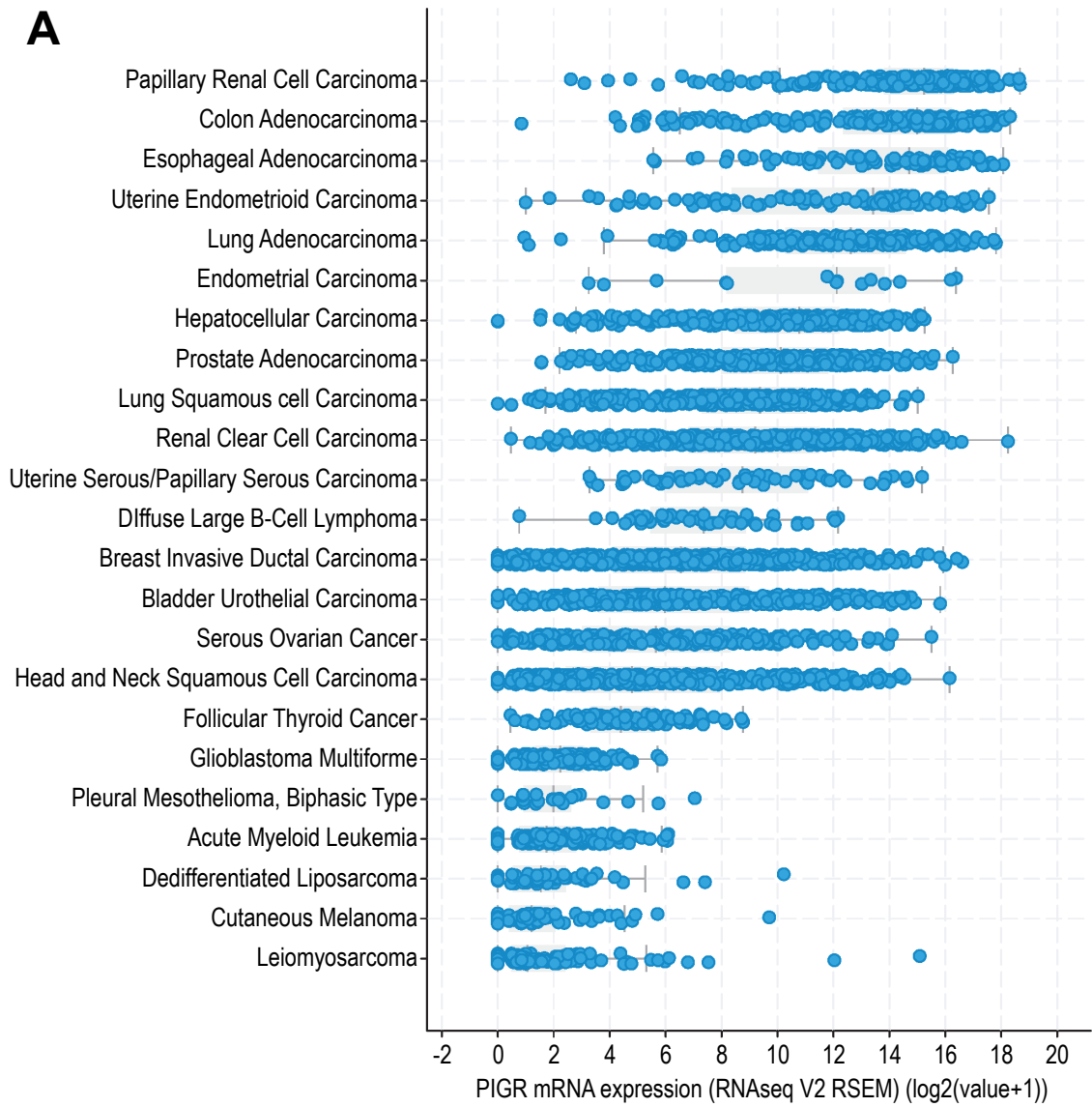
**Supplemental Figure 3, related to Figure 4.** Intratumoral infusion of KRAS<sup>G12D</sup>-specific dIgA1, but not the same antibody on an IgG4 backbone abrogates KRAS<sup>G12D</sup>-OVCAR3, but not KRAS<sup>WT</sup>-OVCAR3 tumor growth, superior to control IgA and MRTX1133, in *Rag1*-deficient mice. (A) Schematic of design of experiment shown in 'B', and 'C'. Antibody (100  $\mu$ g per 20 g body weight) or equal volume of vehicle (PBS) was intratumorally (IT) injected every 4 d, or MRTX1133 (200  $\mu$ g per 20 g body weight) were injected intraperitoneally (IP) every 4 d or daily. (B) Tumor growth curves (*left*), tumor weight (*middle*), tumor volume (*right*) in KRAS<sup>G12D</sup>-OVCAR3 tumor-bearing *Rag1*-deficient mice. Growth curves and tumor weights were pooled from 2 independent experiments ( $n=10$  mice per group, total). (C) Tumor growth curves (*left*), tumor weight (*middle*), tumor volume (*right*) in KRAS<sup>WT</sup>-OVCAR3 tumor-bearing *Rag1*-deficient mice. Growth curves and tumor weights were pooled from 2 independent experiments ( $n=10$  mice per group, total). Data are mean  $\pm$  SEM. \* $P \leq 0.05$ , \*\* $P \leq 0.01$ , \*\*\* $P \leq 0.001$ , NS, not significant; paired two-tailed t-test for growth curves or unpaired two-tailed t-test for tumor weights. **Data S3** provides details of statistics.

**Supplemental Figure 4, related to Figure 4.** Intraperitoneal infusion of KRAS<sup>G12D</sup>-specific dIgA1, but not the same antibody on an IgG4 backbone abrogates KRAS<sup>G12D</sup>-OVCAR3, but not KRAS<sup>WT</sup>- OVCAR3 tumor growth, superior to control IgA and MRTX1133, in NSG mice. (A) Schematic of design of experiment shown in 'B'. Antibody (100 µg per 20 g body weight) or equal volume of vehicle (PBS) every 4 d or MRTX1133 (200 µg per 20 g body weight) every 4 d or daily were injected intraperitoneally (IP). (B) Tumor growth curves (*top*), tumor weight (*bottom left*), representative tumor volume of one experiment (*bottom right*) in KRAS<sup>G12D</sup>-OVCAR3 tumor-bearing NSG mice. Growth curves and tumor weights were pooled from 3 independent experiments ( $n=13$  mice per group, total). Data are mean  $\pm$  SEM. \* $P \leq 0.05$ , \*\*\* $P \leq 0.001$ , NS, not significant; paired two-tailed t-test for growth curves or unpaired two-tailed t-test for tumor weights. **Data S3** provides details of statistics.

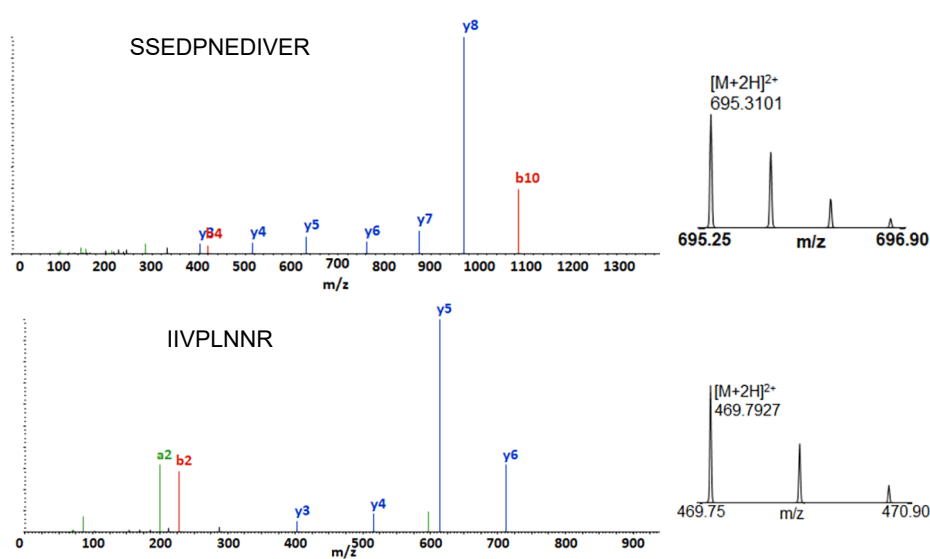
**Supplemental Figure 5, related to Figure 5.** Intraperitoneal infusion of KRAS<sup>G12D</sup>-specific dIgA1, but not the same antibody on an IgG4 backbone abrogates KRAS<sup>G12D</sup> mutated A427 or SK-LU-1 tumors, superior to control IgA and MRTX1133, in NSG mice. (A) Bar graphs showing comparisons of percentages of CD3<sup>+</sup> cells, PIGR<sup>+</sup> cells, IgA-coated cells, and IgG-coated cells within the PCK<sup>+</sup> tumor islets among adenocarcinoma and squamous cell carcinoma histology types. ( $n=12$  each, with two duplicated cores). NS, not significant; Unpaired two-tailed t-test. (B) Schematic of design of experiment shown in 'C' and 'D'. Antibody (100 µg per 20 g body weight) or equal volume of vehicle (PBS) every 4 d or MRTX1133 (200 µg per 20 g body weight) daily or every 4 d were injected IP. (C) Tumor growth curves (*top*), tumor weight (*bottom, left*), tumor volume (*bottom, right*) in A427 tumor-bearing NSG mice. Growth curves and tumor weights were

pooled from 3 independent experiments ( $n=14$  mice per group, total). Data are mean  $\pm$  SEM. \* $P \leq 0.05$ , \*\* $P \leq 0.01$ , NS, not significant; paired two-tailed t-test for growth curves or unpaired two-tailed t-test for tumor weights. **(D)** Tumor growth curves (*top*), tumor weight (*bottom, left*), tumor volume (*bottom, right*) in SK-LU-1 tumor-bearing NSG mice. Growth curves and tumor weights were pooled from 3 independent experiments ( $n=14$  mice per group, total). **(E)** *Left*, schematic design of treatments in KRAS<sup>G12D</sup> Brpkp110 tumor-bearing immunocompetent mice. Antibody (100  $\mu$ g per 20 g body weight) were intraperitoneally injected. *Middle*, tumor growth curves and *right*, tumor weights in mice receiving intraperitoneal anti-KRAS<sup>G12D</sup>-dIgA1, or anti-KRAS<sup>G12D</sup>-IgG4, or non-specific dIgA. Growth curves and tumor weights were pooled from 2 independent experiments ( $n=10$  mice per group, total). Data are mean  $\pm$  SEM. \* $P \leq 0.05$ , \*\* $P \leq 0.01$ , NS, not significant; paired two-tailed t-test for growth curves or unpaired two-tailed t-test for tumor weights. **Data S3** provides details of statistics.

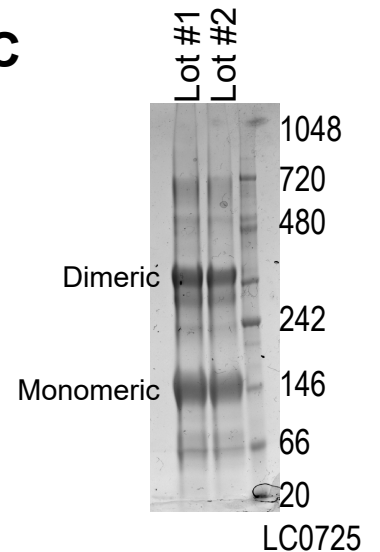
Supplemental Figure 1



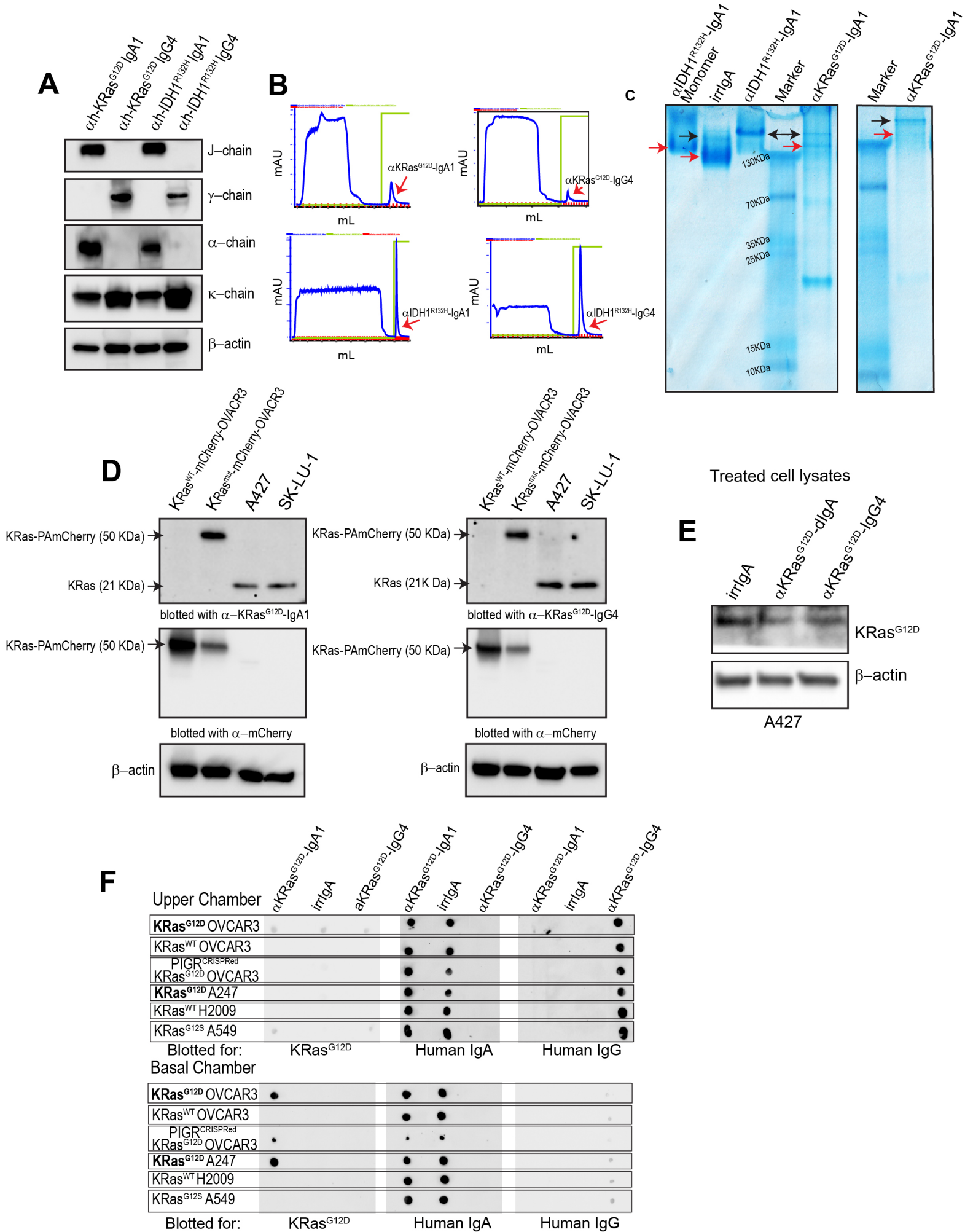
**B**

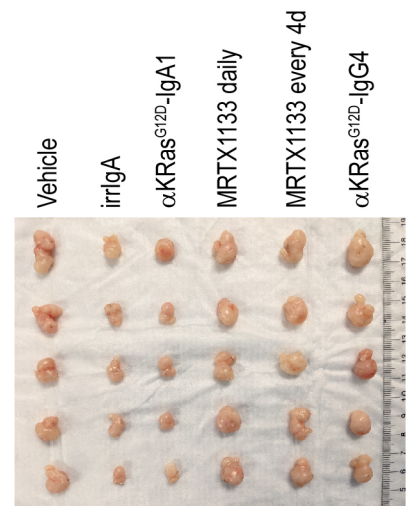
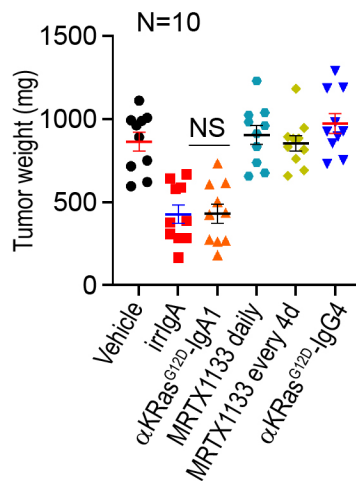
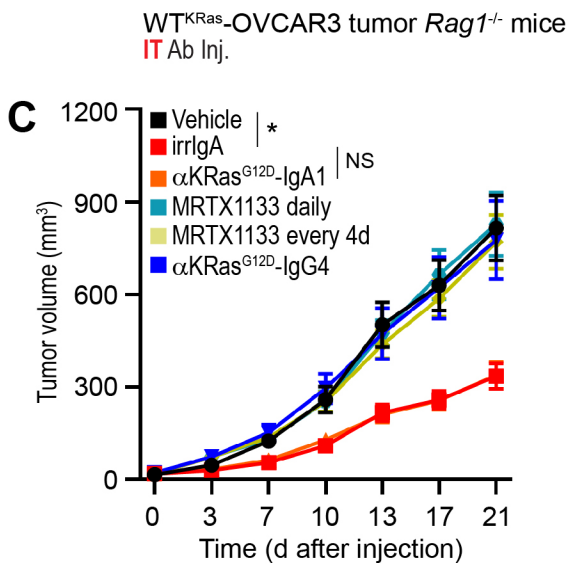
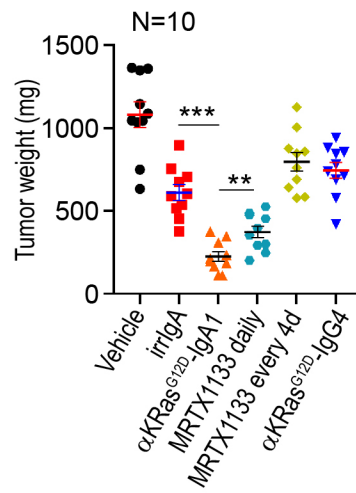
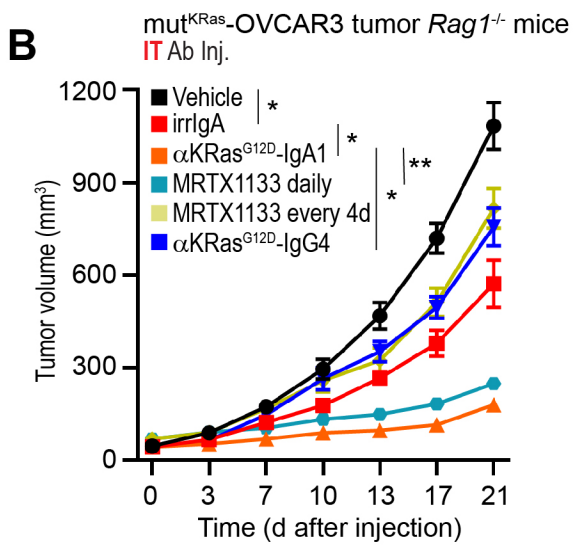
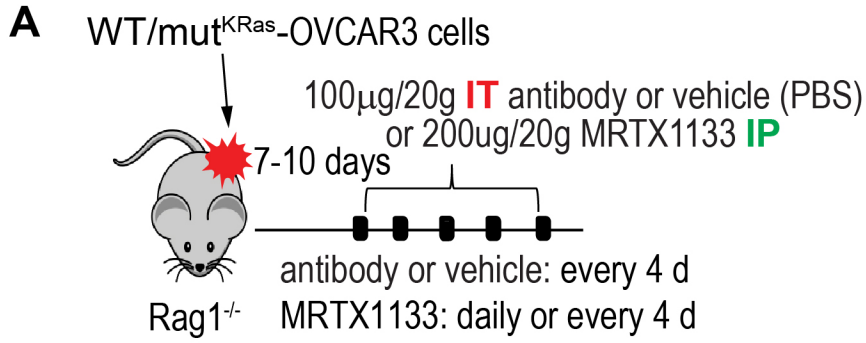


**C**

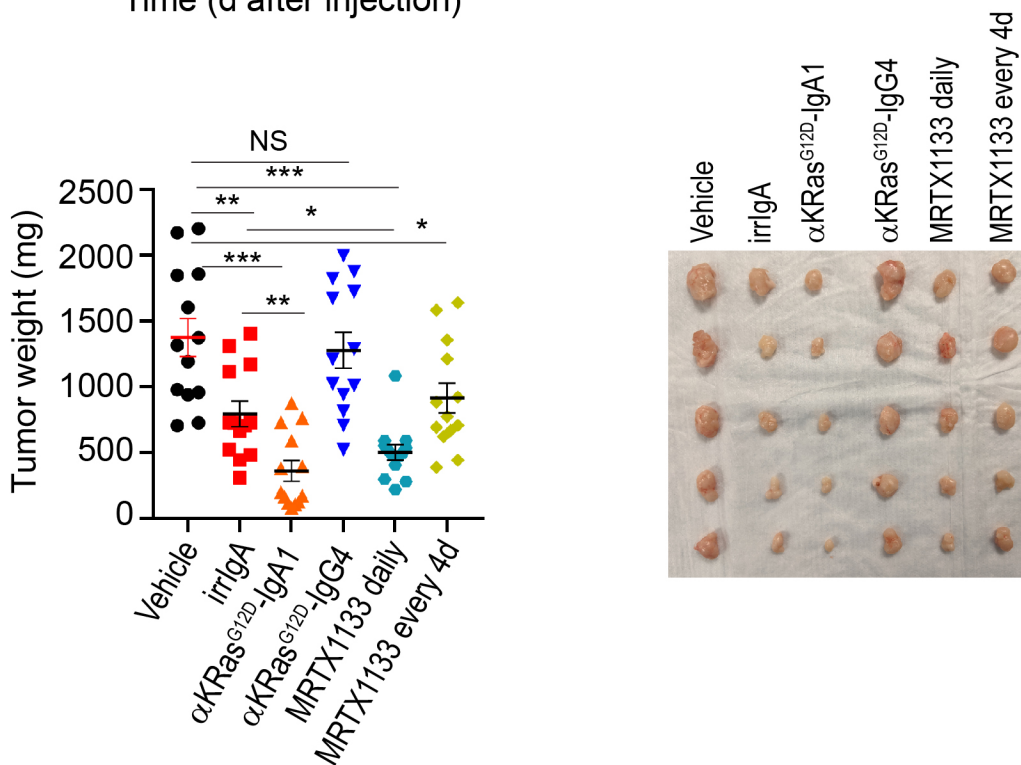
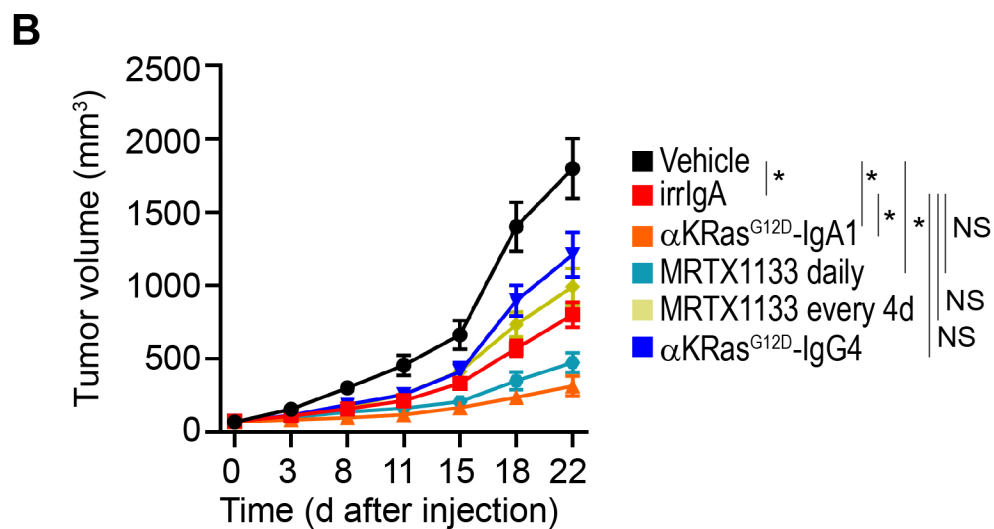
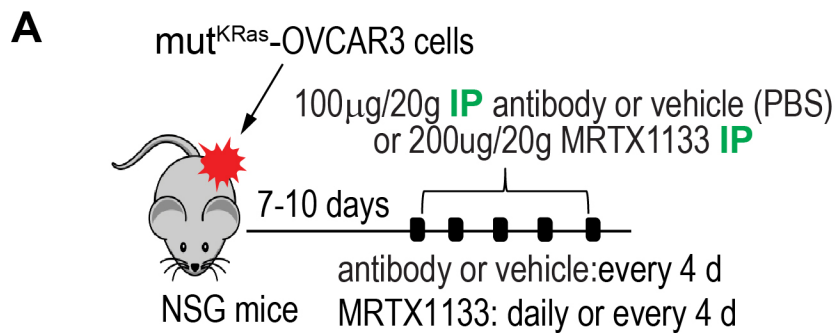


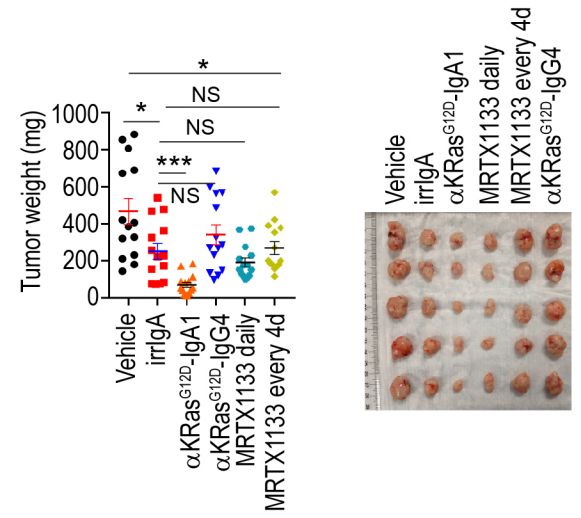
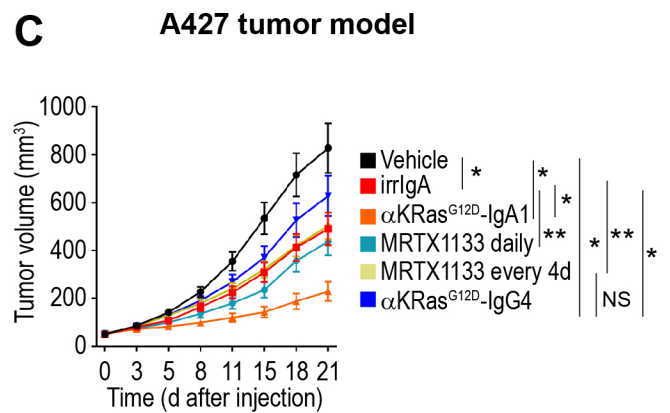
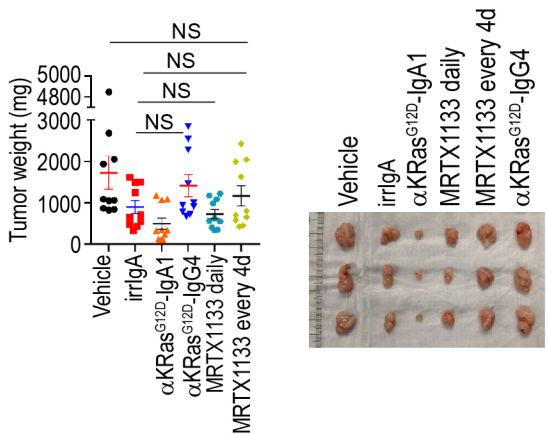
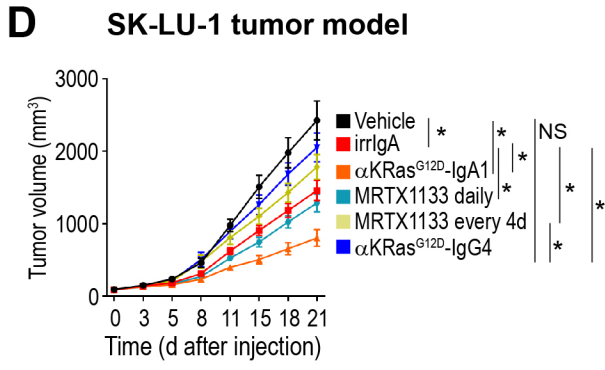
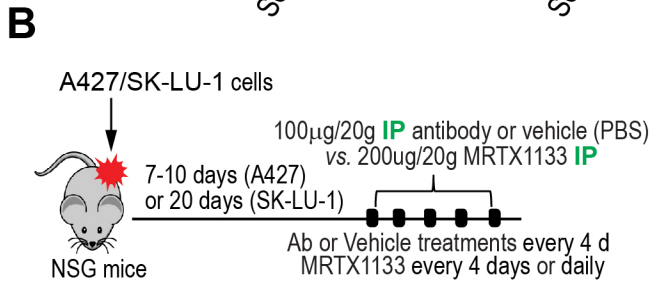
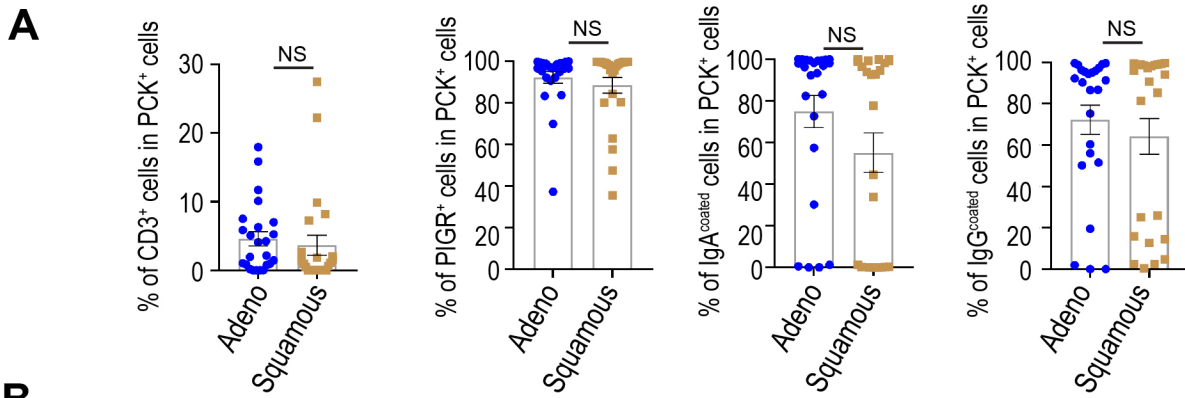
# Supplemental Figure 2





Supplemental Figure 4





**E KRas<sup>G12D</sup>-Brpk110 immunocompetent tumor model**

